Spectroscopic Studies of the Classical Cepheid ζ Gem: Analysis of the Velocity Field in the Atmosphere and Manifestation of the…

Article *in* Astronomy Letters · June 2016

DOI: 10.1134/S1063773716060074

1 author:

Igor A. Usenko

Odessa National University

65 PUBLICATIONS **217** CITATIONS

ISSN 1063-7737, Astronomy Letters, 2016, Vol. 42, No. 6, pp. 393–412. © Pleiades Publishing, Inc., 2016.
Original Russian Text © I.A. Usenko, 2016, published in Pis'ma v Astronomicheskii Zhurnal, 2016, Vol. 42, No. 6, pp. 437–457.

Spectroscopic Studies of the Classical Cepheid ζ Gem: Analysis of the Velocity Field in the Atmosphere and Manifestation of the Presence of a Circumstellar Envelope

I. A. Usenko*

Astronomical Observatory, Odessa National University, Shevchenko Park, Odessa, 65014 Ukraine

Received December 21, 2015

Abstract—Based on five high-resolution spectra in the range 5625–7525 Å taken in 1995 and covering the ascending branch of the light curve from minimum to maximum, we have performed spectroscopic studies of the classical Cepheid ζ Gem. The atmospheric parameters and chemical composition of the Cepheid have been refined. The abundances of the key elements of the evolution of yellow supergiants are typical for an object that has passed the first dredge-up: a C underabundance, N, Na, and Al overabundances, and nearly solar O and Mg abundances. We have estimated [Fe/H] = +0.01 dex; the abundances of the remaining elements are also nearly solar. The metal absorption lines in all spectra show a clear asymmetry and the formation of secondary blue (B1 and B2) and red (R1 and R2) components, just as for the Cepheid X Sgr. The Hα absorption line is also split into blue (B) and red (R) components with different depths changing with pulsation phase. To analyze the velocity field in the atmosphere of ζ Gem, we have estimated the radial velocities from specially selected (with clear signatures of the B1, B2, R1, and R2 components) absorption lines (neutral atoms and ions) of metals (38 lines) and the B and R components of the Hα line. Analysis of these estimates has shown that their scatter is from −22 to 36 km s^{-1} for all pulsation phases but does not exceed 35–40 km s^{-1} for each individual phase, while it does not exceed 22 km s^{-1} for the Hα line components. The radial velocity estimates for the metal lines and their B1 and B2 components have been found to depend on the depths, suggesting the presence of a velocity gradient in the atmosphere. No significant difference in velocities between the atoms and ions of the metal lines is observed, i.e., there is no significant inhomogeneity in the upper atmospheric layers of the Cepheid. Since the averaged radial velocity estimates for the cores of the metal lines and their B1 and B2 components change with pulsation phase and coincide with those for the B component of the Hα line, they are all formed in the Cepheid's atmosphere. The formation and passage of a shock wave due to the κ-mechanism at work can be responsible for the stronger scatter of the B1 and B2 components in their velocities at phases after the Cepheid's minimum radius. The averaged velocities of the R1 components also change with pulsation phase and differ only slightly from the remaining ones. On the other hand, the mean velocity estimate for the R component of the Hα line at all phases is $+32.72 \pm 2.50$ km s^{-1} and differs significantly from the bulk of the velocities, suggesting the formation of this component in the envelope around the Cepheid. The unusual behavior of the mean velocities for the R2 components of the metal absorption lines can also point to their formation in the envelope and can be yet another indicator of its presence around ζ Gem.

DOI: 10.1134/S1063773716060074

Keywords: *Galactic Cepheids, optical spectra, atmospheric parameters, chemical composition, secondary components of metal absorption lines, splitting of hydrogen absorption lines, radial velocities, gaseous circumstellar envelopes.*

INTRODUCTION

The classical Cepheid ζ Gem is one of the brightest and interesting representatives of this class of pulsating variable yellow supergiants in the Galaxy. Having a pulsation period of $10^{d}.15$ (Kholopov et al. 1986), the variable is between the classical Cepheids (DCEP) with pulsation periods from 7^{d} to 9^{d} (for which a characteristic secondary maximum or a "crest" beginning from the minimum and approaching the maximum as the pulsation period increases is observed on the descending branch of the light, color, and radial velocity curves) and the objects with pulsation periods longer than 10^{d} (when the crest is displaced from maximum to minimum along the ascending branch of the light, color, and radial

*E-mail: igus99@ukr.net

velocity curves). The coincidence of the primary and secondary maxima in ζ Gem imparts a nearly sinusoidal shape to these curves, just as for small-amplitude Cepheids (DCEPS); therefore, some authors assign the variable to this class. ζ Gem is also a calibration object for the period–luminosity–color (P–L–C) relation.

While investigating the behavior of the radial velocity curves for the Cepheid measured from metal absorption lines and Hα, Jacobsen and Wallerstein (1982) detected a significant positive displacement of the latter, just as for the shorter-period Cepheid η Aql ($P = 7^{\rm d}$) and the longer-period X Cyg ($P = 16^{\rm d}$). Such a phenomenon for three Cepheids with pulsation periods close to $10^{\rm d}$ (S Mus, β Dor, and S Nor) was detected previously by Rogers and Bell (1967a, 1967b) and Schmidt (1970). Jacobsen and Wallerstein (1982) pointed out that the H_α line shows a strong asymmetry with a red core and a blueshifted wing, while the displacement between the radial velocity curves measured from the iron and Hα lines is 9 km s^{-1} or about $0\overset{P}{.}2$ of the phase cycle. The authors gave a possible explanation for this phenomenon: the appearance of a wave reflected from the upper chromosphere that provides some combination of compression, recombination, and downward velocity in the stellar atmosphere. Nardetto et al. (2008) showed the peculiar behavior of the Hα line to be very typical for Cepheids with periods longer than $10^{\rm d}$ and offered the version that this effect could be due to the presence of an extended circumstellar envelope. Kervella and Dominicano de Souza (2006), Mérand et al. (2006, 2007), Barmby et al. (2011), and Gallenne et al. (2012) (the observations of Cepheids on the FLUOR infrared interferometer, the Spitzer Space Telescope, and the VISIR infrared photometer) confirmed the presence of such envelopes around many Cepheids (in particular, around the above-mentioned S Mus, X Cyg, and η Aql).

While investigating high-resolution spectra for the peculiar Cepheid X Sgr ($P = 7^{\rm d}$), Mathias et al. (2006) detected a multicomponent structure in the metal absorption lines, i.e., the presence of two or three red and/or blue components in each line, depending on the pulsation phase. The authors interpreted this phenomenon as a manifestation of two consecutive shock waves in the atmosphere, one being apparently related to the so-called κ-mechanism at work, while the origin of the second shock was unclear. After the detection of a circumstellar envelope of gas and dust around X Sgr (Gallenne et al. 2012), Usenko et al. (2013) suggested that its presence could explain the multicomponent structure of the metal absorption lines. In this and subsequent papers (Usenko et al. 2014a, 2014b; Usenko and Klochkova 2015), by analyzing the anomalous behavior of the Hα, Hβ, and metal absorption lines, it was concluded that such envelopes could be present not only around long-period Cepheids (SZ Cas, RU Sct) but also around short-period ones (Y Sgr, BG Cru, AV Cir, BP Cir, LR TrA, BY Cas). Thus, taking into account the anomalous behavior of the Hα line in ζ Gem, it is suggested that a circumstellar envelope may be present around this Cepheid.

OBSERVATIONS AND PRIMARY REDUCTION

In this paper, we used five spectra of ζ Gem taken in September 1995 with the Coudé spectrograph of the Kitt Peak National Observatory (Fry and Carney 1997) and provided by B. Carney. The resolution is $R \approx 30\,000$, the signal-to-noise ratio is S/N = 167–180 for 18 spectral orders in the spectral range 5625–6890 Å with a length of each from ≈75 to ≈90 Å and one order 7425–7525 Å with a length of 100 Å. The spectra were taken in an interval of seven consecutive nights. According to the data of the above authors, this allowed half of the pulsation period from minimum to maximum light to be covered.

The primary image reduction was performed with the IRAF software package. The spectra were converted to the format of the DECH 20 software package (Galazutdinov 1992), which was used to measure the absorption line equivalent widths and radial velocities. The Julian dates of the observations were taken from Fry and Carney (1997), while the pulsation phases were calculated using the ephemerides from Kiss (1998) and are presented in Tables 1 and 3. Due to their significant asymmetry and the multicomponent structure of individual lines, the equivalent widths of the metal absorption lines were measured mostly by direct integration and, in rare cases, by Gaussian fitting.

DETERMINATION OF THE ATMOSPHERIC PARAMETERS AND CHEMICAL COMPOSITION

To determine the effective temperature, Fry and Carney (1997) used the $(B-V)$–$T_{\rm eff}$ relation for Cepheids (Fry and Carney 1999) followed by its improvement according to the spectroscopic criterion for the neutral iron abundance being independent of the lower-level excitation potential. The values of $\log g$ and V_t were determined from the equality of the abundances derived from Fe I and Fe II lines and from the absence of any dependence of the Fe I abundances

Table 1. Atmospheric parameters of ζ Gem for each spectrum

HJD 2440000+	Phase	This paper			FC97*		
		$T_{\rm eff}$, K	$\log g$	V_t, km s^{-1}	$T_{\rm eff}$, K	$\log g$	V_t, km s^{-1}
9981.9975	0.495	5229 ± 6	1.40	4.10	5250 ± 50	1.50	3.40
9982.9872	0.593	5344 ± 10	1.40	4.70	5310 ± 50	1.50	2.90
9985.0197	0.793	5694 ± 8	1.60	4.50	5675 ± 50	1.70	3.30
9986.0172	0.891	5748 ± 6	1.70	4.50	5750 ± 50	1.70	3.20
9987.0040	0.988	5847 ± 7	1.90	4.60	5875 ± 50	2.00	3.30

* FC97 stands for Fry and Carney (1997).

on their equivalent widths, respectively. For comparison, these estimates are given in columns 6–8 of Table 1. In this paper, we used more perfect methods for determining the atmospheric parameters of ζ Gem using spectroscopic criteria.

(1) The effective temperature $T_{\rm eff}$ was determined from the depth ratios of the lines of iron-peak elements for pairs of lines with different excitation potentials calibrated by Kovtyukh (2007). The accuracy of the temperature is 6–10 K.

(2) The surface gravity $\log g$ was determined from the condition for the abundances derived from Fe I and Fe II lines being equal. The mean accuracy of this parameter is 0.15 dex.

(3) The microturbulent velocity V_t was determined from the condition for the Fe II abundance being independent of the line equivalent width W_λ. Its mean accuracy is 0.25 km s^{-1}.

We computed the model atmospheres and chemical composition for each spectrum using a version of the WIDTH9 code based on the grid of models by Kurucz (1992) with the solar estimates of $\log gf$ taken from Kovtyukh and Andrievsky (1999). The derived atmospheric parameters are presented in Table 1. For our analysis, we used lines with equivalent widths of no more than 160 mÅ, because large errors are possible for stronger lines due to the inaccuracy of the damping constants.

Table 2 presents the estimated elemental abundances relative to the Sun [El/H] with their errors σ and gives the number of lines NL used for a given element. For comparison, column 5 gives the averaged elemental abundances from Luck et al. (2008). Complete information about the influence of uncertainties in determining the atmospheric parameters on the elemental abundance estimates is described in Berdnikov et al. (2010). For the elements with a hyperfine line structure , we used the values of $\log gf$ obtained by summing all oscillator strengths for a given line. As is pointed out in Berdnikov et al. (2010), given the accuracy of the parameter determination and the equivalent width measurement, the mean error of their abundances for supergiants is 0.2–0.3 dex.

SPECTRAL ABSORPTION LINES AND RADIAL VELOCITY MEASUREMENTS

Based on IUE ultraviolet spectra, Schmidt and Parsons (1984) detected deep blueshifted absorptions in the emission components of the Mg II h and k resonance lines for the Cepheid. They explained this phenomenon as an intense mass loss from the surface (stellar wind) and estimated it to be 10^{-10} $M_\odot$. Subsequently, Deasy (1988) showed that such a stellar wind could be detected by blueshifted absorption dips not only in the Mg II h and k lines but also in the Ca II H and K lines as well as in Hα. Since the Mg II h and k lines are good indicators of circumstellar absorption and the possible presence of an envelope and since the velocities measured from the blueshifted absorptions lie within the range from -120 to -160 km s^{-1} (depending on the pulsation cycle), the mass of the possible envelope estimated from them was $\sim 2.5 \times 10^{-10}$ $M_\odot$, while the mass loss was 10^{-10} $M_\odot$. While analyzing the spectra of ζ Gem taken in the infrared range 10 800–16 000 Å, Sasselov and Lester (1990) detected an asymmetry of the photospheric absorption lines in it (just as in other seven investigated Cepheids except for α UMi).

Table 2. Elemental abundances in the atmosphere of ζ Gem

Species	This paper			LAFK08*
	[El/H]	σ	NL	[El/H]
C I	−0.29	0.13	28	−0.22
N I	+0.45	0.11	10	−
O I	−0.04	0.07	14	−0.05
Na I	+0.21	0.09	11	+0.24
Mg I	−0.06	0.13	12	−0.09
Al I	+0.17	0.11	10	+0.12
Si I	+0.03	0.09	109	+0.02
Si II	+0.30	0.03	5	+0.18
S I	+0.12	0.18	27	+0.07
Ca I	−0.08	0.09	25	−0.07
Sc I	+0.11	0.12	10	+0.10
Sc II	−0.20	0.05	10	+0.05
Ti I	−0.00	0.13	98	+0.00
Ti II	−0.01	0.05	5	−0.02
V I	−0.01	0.09	72	−0.02
V II	−0.13	0.09	10	−0.13
Cr I	−0.03	0.115	52	−0.02
Cr II	+0.20	0.11	5	+0.13
Mn I	−0.18	0.09	17	+0.03
Fe I	+0.01	0.10	593	+0.01
Fe II	+0.01	0.07	112	+0.02
Co I	−0.16	0.06	40	−0.16
Ni I	−0.12	0.10	174	−0.01
Cu I	−0.06	0.09	9	−0.02
Zn I	+0.20	0.16	5	+0.20
Y I	+0.39	0.15	6	+0.25
Y II	+0.18	0.05	9	+0.21
Zr II	−0.18	0.17	8	−0.09
Ru I	−0.38	0.15	3	−
La II	+0.15	0.11	10	+0.14
Ce II	−0.07	0.06	9	−0.11
Nd II	+0.04	0.22	15	+0.04
Eu II	+0.03	0.09	10	+0.05
Gd II	−0.16	0.13	5	+0.00

* LAFK08 stands for Luck et al. (2008).

The asymmetry manifested itself on both blue and red sides of the lines: as an example, the Si I 10844 Å and C I 10707 Å lines were shown at phases $0^P.27$ and $0^P.77$, respectively (see Figs. 4 and 5 from their paper). However, the appearance of additional absorption line components, as in X Sgr, δ Cep, and η Aql, was not recorded in ζ Gem. As has already been mentioned in the Introduction, a multicomponent structure and an absorption line asymmetry at optical wavelengths as well as the presence of envelopes are typical for these three Cepheids.

A visual estimate of the five spectra used in this paper suggests that a multicomponent structure of the absorption lines, which is so prominent, for example, in X Sgr, is also present here: the secondary components appear and disappear on both blue and red sides of the line for both neutral atoms and ions, depending on the pulsation phase (see Figs. 1–3), and with different values of $\chi_{\rm low}$ (Fig. 4). However, the most interesting fact is that in ζ Gem, just as in X Sgr (Mathias et al. 2006), the secondary components are split into two components, with this phenomenon being most pronounced in weak lines (Fig. 5). The strong Na I D resonance lines also exhibit blue and red components (Fig. 6).

The Hα absorption line profile also looks unusual: its splitting into two components is noticeable, with the line core being shifted from the blue region to the red one with rising effective temperature due to the change in pulsation phase (Fig. 7).

To investigate the dynamical processes in the atmosphere and envelope of the yellow hypergiant ρ Cas, Klochkova et al. (2014) used the radial velocities measured not only from the cores of the hydrogen and metal absorption lines but also from the blue and red components of these lines. Particular attention was given to the lines of neutral atoms and ions with low lower-level excitation potentials $\chi_{\rm low}$ and to the Na I D resonance lines. Therefore, in this case with ζ Gem, the same technique but with some distinctions was used. The bulk of the radial velocities were estimated from the cores of the metal absorption lines and Hα (see Table 3). In contrast, the so-called anomalous lines, unblended ones, with a clear presence of such components (preference was given to the lines where two or three components were present, depending on the pulsation phase) and with different intensities were selected for the estimates from the blue and red components. Apart from the Hα absorption line, a total of 38 such anomalous lines of neutral atoms and ions of metals were selected in the range 5625–6800 Å (see Table 4). As can be seen from Table 4, there are lines not only with low values of $\chi_{\rm low}$ but also with high ones in this list. Apart from the radial velocity estimates, the

Table 3. Radial velocities of ζ Gem for each spectrum determined from the metal absorption lines and Hα profile components

HJD 2440000+	Phase	Metal lines			Hα					
		RV, km s^{-1}	σ, km s^{-1}	NL	RV_B, km s^{-1}	r	RV_C, km s^{-1}	r	RV_R, km s^{-1}	r
9981.9975	0.495	20.88	1.01	399	6.82	0.669	22.59	0.632	32.33	0.568
9982.9872	0.593	12.28	1.13	332	3.75	0.666	13.59	0.662	32.57	0.607
9985.0197	0.793	4.09	0.81	355	−5.83	0.602	4.09	0.651	37.17	0.767
9986.0172	0.891	2.20	0.73	348	−13.43	0.594	3.34	0.647	32.11	0.710
9987.0040	0.988	0.07	1.01	339	−15.31	0.609	−0.05	0.651	29.41	0.666

NL is the number of lines, r is the depth of the Hα line components, RV_B—from the blue line component, RV_C—from the line center, RV_R—from the red line component.

depths were also measured for these lines and their components. The same procedure was also performed for Hα (Table 3). Tables 5–9 present these values for each of the five spectra, where column C gives the estimates from the line core, columns B1 and B2 give the estimates from the blue components located closer to and farther from the line core, respectively, and columns R1 and R2 give the estimates from the red components located closer to and father from the line core, respectively.

DISCUSSION

Atmospheric Parameters and Chemical Composition

It can be seen from the results obtained in this paper that the Cepheid's derived atmospheric parameters (Table 1) $T_{\rm eff}$ and $\log g$ differ only slightly from those in Fry and Carney (1997), while this difference for V_t is more significant. As regards the elemental abundances in the atmosphere of ζ Gem (Table 2), the results from Luck et al. (2008) were used for comparison, because Fry and Carney (1997) did not provide detailed estimates for each element. Only the mean abundance estimates, $[{\rm Fe/H}] = +0.00 \pm 0.04$ dex and $[\alpha/{\rm Fe}] = +0.07 \pm 0.03$ dex, were presented. Luck et al. (2008) estimated the abundance of 25 elements, with the exception of nitrogen and ruthenium.

It can be seen from Table 2 that the abundances of the key elements of the evolution of yellow supergiants in the atmosphere of ζ Gem are typical for a Cepheid that has passed the first dredge-up: a carbon underabundance, nitrogen, sodium, and aluminum overabundances, and solar oxygen and magnesium abundances. The abundances of the α-elements, Fe-peak elements, and r- and s-process elements are also nearly solar. There is good agreement of our estimated with the results of Luck et al. (2008).

Analysis of the Velocity Field in the Cepheid's Atmosphere and the Presence of a Circumstellar Envelope

As the Cepheid's mean radial velocity, we used the estimate of $\langle V_r \rangle = +6.7$ km s^{-1} taken from the catalog of Wielen et al. (1999). Since $\langle V_r \rangle$ changes within 1 km s^{-1}, it was chosen closer to the date at which the spectra were taken. To analyze the velocity field, we used the graphs of the dependence of the radial velocity estimates on line depth (Tables 5–9) and the change of the radial velocities estimated from the cores of the metal absorption lines, their blue and red components, and the Hα line components (Fig. 8) as well as the dependence of the averaged velocity estimates for these lines and their components on pulsation phase (Fig. 9). It follows from these tables and figures that the scatter in velocities is from −22 to +36 km s^{-1} for all pulsation phases, which is quite significant (for the hypergiant ρ Cas, it is from −10 to −70 km s^{-1} (Klochkova et al. 2014)), but it does not exceed 35–40 km s^{-1} for each individual phase, except for the Hα line components. It is best to consider the behavior of the radial velocity estimates for each individual spectrum. For comparison, we used the curve of radius variation for the Cepheid from Russo and Sollazzo (1980).

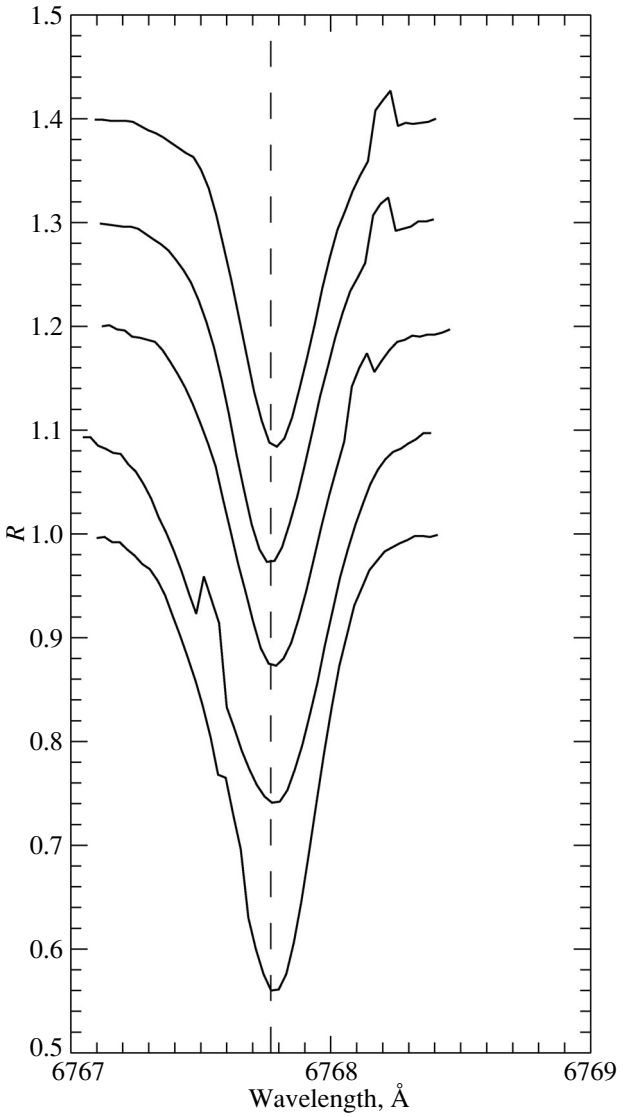

Fig. 1. Changes of the Cr I 6767.770 Å ($\chi_{low} = 1.83$ eV) absorption line profile with increasing pulsation phase (from bottom to top).

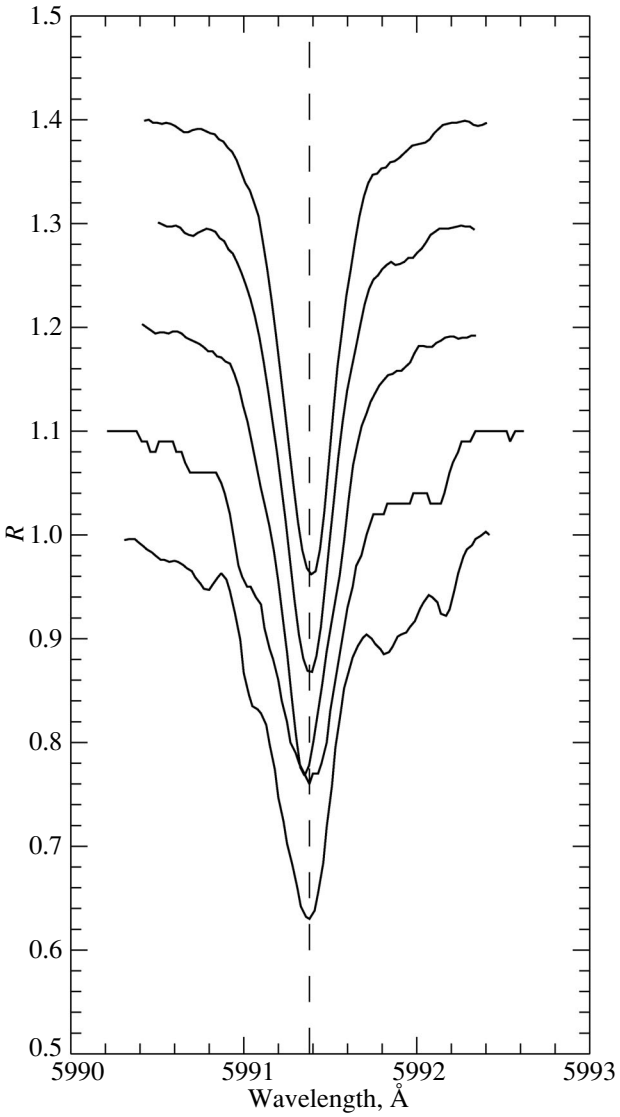

Fig. 2. Changes of the Fe II 5991.375 Å ($\chi_{low} = 3.15$ eV) absorption line profile with increasing pulsation phase (from bottom to top).

(1) **Phase $0^P.495$.** The time of minimum light, when the Cepheid was contracting and its radius decreased approximately by a quarter of the maximum value. As can be seen from the graph in Fig. 8, there is some dependence of the radial velocities measured from the cores of the metal lines on the depth of these lines, with no significant difference between the neutral atoms and ions being observed. The same dependence is also typical for the B2 components and is very weak for the B1 components. The R2 components are farthest from the bulk of the lines in the red region, and the velocity difference exceeds 15 km s^{-1}. The R2 component of the Na I D 5889.966 Å resonance line shows the greatest "red" velocity close to the R component of the Hα line, and two strong B1 components are present in both doublet lines. There are a total of three R1 components, and the existence of such a dependence cannot be judged from them. On the other hand, the velocity of the B component of the Hα line coincides with $\langle V_r \rangle$. It can be seen from Fig. 9 that the averaged velocity of the B2 components also coincides with the estimate from the B component of the Hα line and with $\langle V_r \rangle$. At the same time, the averaged velocity from the R2 components coincides closely with the radial velocity estimated from the R component of the Hα line. The depth of the B

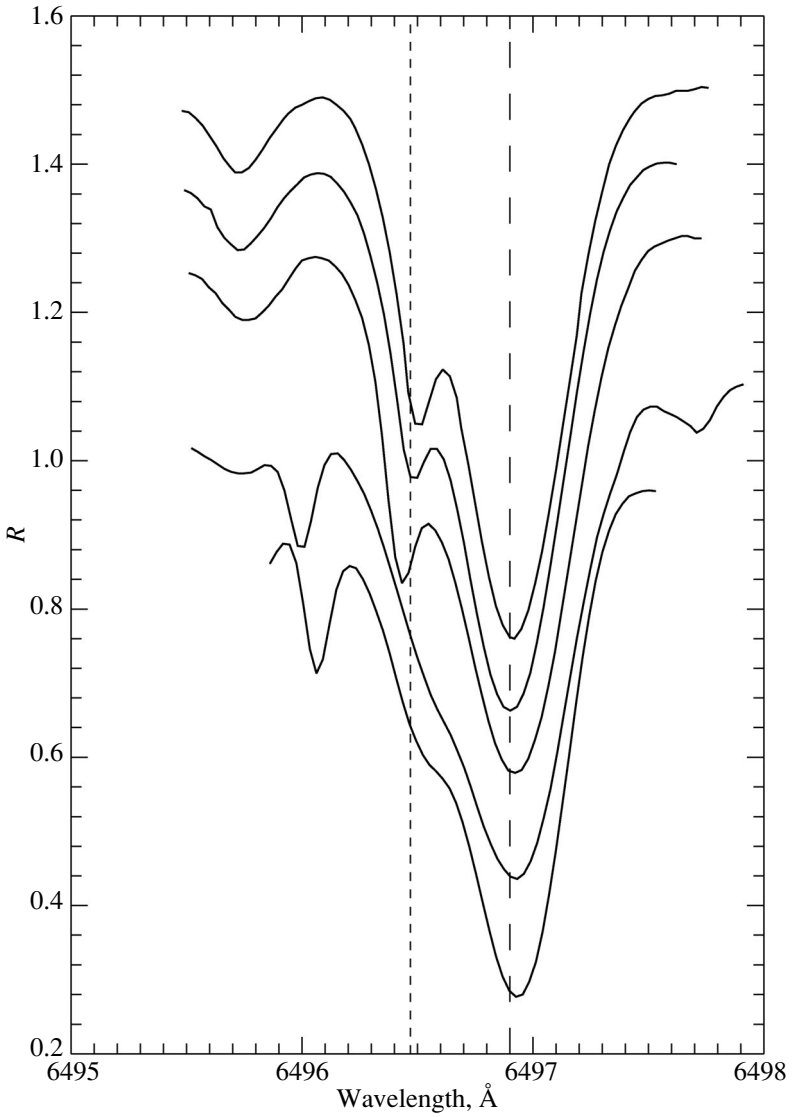

Fig. 3. Changes of the Ba II 6496.910 Å ($\chi_{low} = 0.60$ eV) absorption line profile with increasing pulsation phase (from bottom to top).

component of the Hα line exceeds the depth of its R component. In total, the number of components at this phase is: 30 B1 (maximum number), 19 B2, 3 R1 (minimum number), and 8 R2.

(2) **Phase $0^P.593$.** This spectrum corresponds exactly to the mean radius of the Cepheid. There is further contraction. The dependence of the radial velocities on line depth becomes less pronounced when estimated from the metal line cores and is virtually absent when estimated from the B1 and B2 components (see Fig. 8). The R1 components approach the R2 components. The difference in velocity for the latter from the bulk of the lines decreases: the R2 components are blueshifted approximately by 10 km s^{-1}. Only strong B1 components are observed in the Na I D resonance lines. There is a large blue shift of the B component of the Hα line. It can be seen from Fig. 9 that the approach of this B component to the mean velocity for the B1 component, which, in turn, approaches $\langle V_r \rangle$, is characteristic for this phase. On the other hand, the velocity for the R component of the Hα lines remains essentially unchanged. The depth of the B component of the Hα line approaches that for the R component. In total, the number of components at this phase is: 18 B1, 29 B2 (maximum number), 6 R1, and 5 R2 (minimum number).

(3) **Phase $0^P.793$.** The minimum radius is the maximum contraction of the Cepheid's atmosphere.

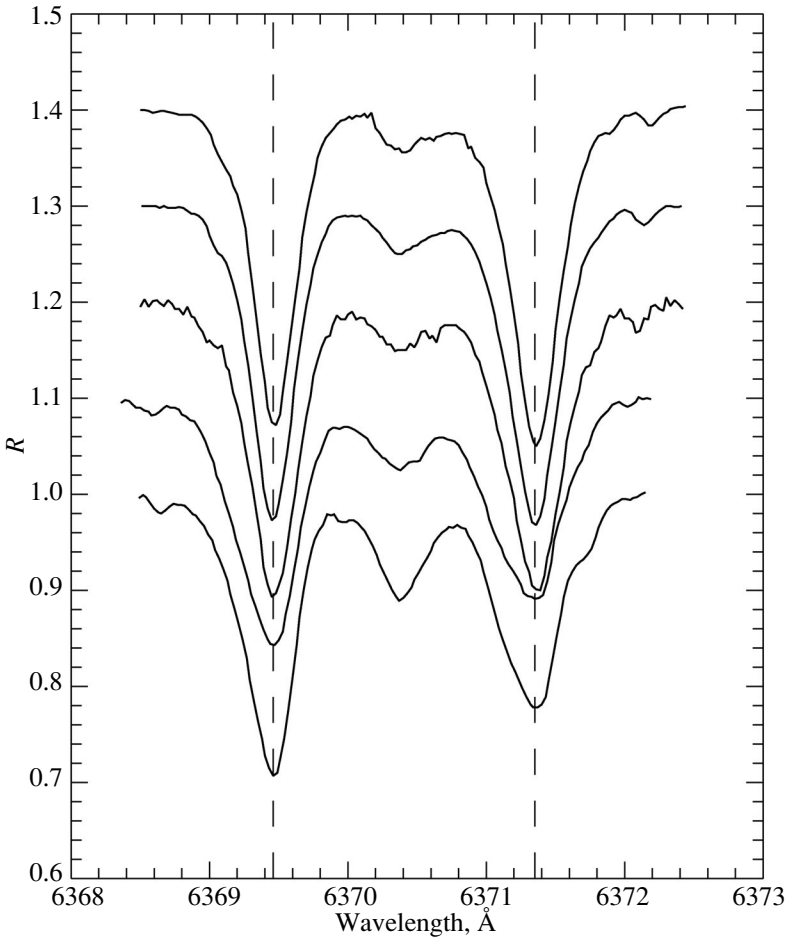

Fig. 4. Changes of the Fe II 6369.460 Å ($\chi_{low} = 2.89$ eV) and Si II 6369.460 Å ($\chi_{low} = 8.12$ eV) absorption line profiles with increasing pulsation phase (from bottom to top).

The radial velocities determined from the metal line cores are close to $\langle V_r \rangle$. The B1 and B2 components are blueshifted further, with the scatter in velocities for the B2 components increasing ($\sim$10 km s^{-1}); the R2 components also continue to be blueshifted and approach the R1 components. As in the previous case, there are only strong B1 components in the Na I D resonance lines. There is no apparent dependence of the radial velocities estimated from the cores of the metal lines and their components on line depth either. The depth of the R component of the Hα line and its velocity reach their maximum values, while the B component continues to be blushifted further (Fig. 8). Remarkably, the velocity estimate for the B component of the Hα line is intermediate between the averaged velocity estimates for the B1 and B2 components (Fig. 9). The averaged velocity estimate for the R1 component is close to $\langle V_r \rangle$. In total, the number of components at this phase is: 27 B1, 12 B2, 17 R1, and 8 R2.

(4) **Phase $0\overset{P}{.}891$.** The stage of expansion of the Cepheid's atmosphere and further increase in its radius. A slight dependence of the radial velocities estimated from the metal line cores on line depth begins to manifest itself. The same can also be said about the B1 components, though an increase of the scatter in velocities to 10 km s^{-1} is noticeable from them. The same scatter in velocities is also noticeable for the B2 components. These components reach their maximum blueshift. The R1 and R2 components show no such dependence, while the averaged velocity estimate for the R1 components coincides with $\langle V_r \rangle$ (Fig. 8). The velocity difference between the R1 and R2 components remains approximately the same as that at the previous phase; their mean values change insignificantly. A strong B1 component is observed in the Na I D 5889.966 Å resonance line, and a strong R1 component is observed in the 5895.932 Å line. At this phase, the velocity of the B component of the Hα line coincides with the averaged velocity estimate for

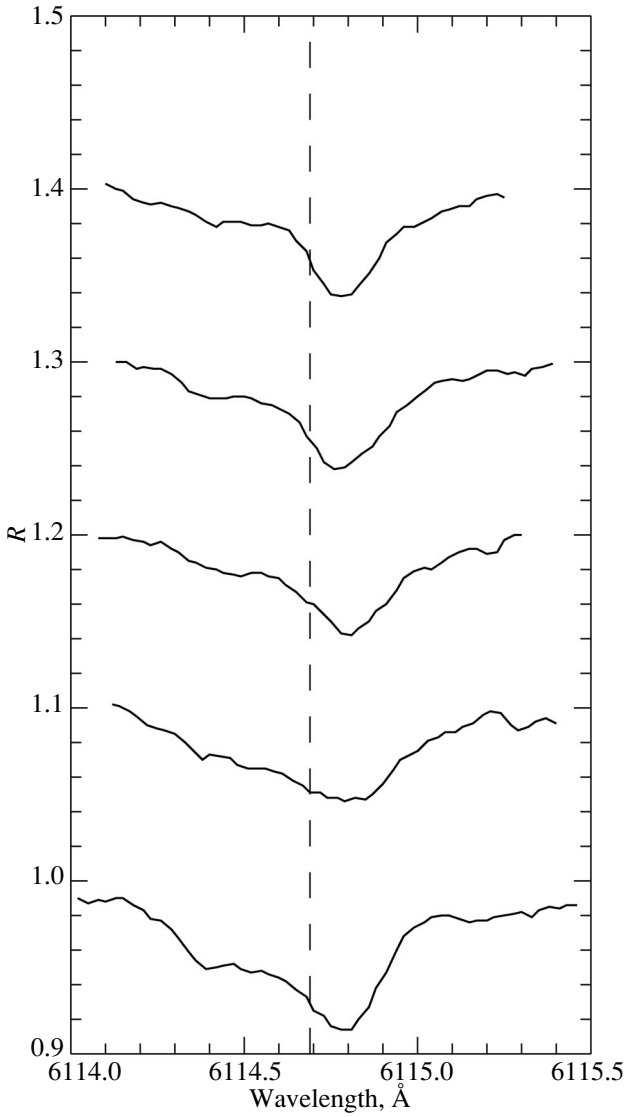

Fig. 5. Changes of the Zr II 6114.690 Å ($\chi_{low} = 1.66$ eV) absorption line profile with increasing pulsation phase (from bottom to top).

the B2 component, while the velocity of the R component of the Hα line is approximately equal to those at phases $0\overset{P}{.}495$ and $0\overset{P}{.}593$ (Fig. 9). The depth of the R component continues to decrease; the difference in depth for both components also decreases. In total, the number of components at this phase is: 25 B1, 9 B2 (minimum number), 19 R1 (maximum number), and 10 R2.

(5) **Phase $0\overset{P}{.}988$.** Maximum light, the Cepheid's atmosphere continues to expand, and its radius increases approximately by a quarter. The slight dependence of the radial velocities estimated from the metal line cores on line depth that manifested itself at the previous phase persists; it is unnoticeable for the B1 components. The scatter in velocities for the B2 components is retained as before, and they show a maximum blueshift as before. The positions of the R1 and R2 components remain virtually the same as do their averaged velocity estimates, and the mean velocity of the R1 component also coincides with $\langle V_r \rangle$ (Fig. 8). On the other hand, only two strong R1 components are observed in the Na I D lines. The coincidence of the velocity for the B component of the Hα line with the averaged velocity estimate for the B2 components is retained (Fig. 9). The velocity of the R component of the Hα line slightly decreases, its depth also decreases, while it increases for the B component. In total, the number of components at this phase is: 12 B1 (minimum number), 11 B2, 17 R1, and 12 R2 (maximum number).

Thus, the revealed dependence of the radial velocities measured from the cores of the metal lines and their B components on line depth suggests the presence of a velocity gradient in the Cepheid's atmosphere. This dependence is observed at the times of contraction of the atmosphere to its minimum radius and subsequent expansion. Such a dependence was occasionally observed in the atmosphere of the hypergiant ρ Cas (Klochkova et al. 2014) and was also explained by variability due to pulsational activity. Nevertheless, in contrast to ρ Cas, no significant difference in the velocities measured from the lines of neutral atoms and ions is observed in ζ Gem. Consequently, in the outer atmospheric layers of the Cepheid, there is no significant inhomogeneity, as in ρ Cas.

The mean radial velocities of the B1 and B2 components are seen to change with pulsation phase similarly to the velocities measured from the metal line cores. The coincidences of the averaged velocity estimates for the B1 and B2 components (including the components of the Na I D resonance lines) with the velocities of the B component of the Hα line at all five pulsation phases show that all these components are formed in the Cepheid's atmosphere (Fig. 9). The formation and passage of a shock wave due to the κ-mechanism at work, which was written about by Mathias et al. (2006), can be responsible for the decrease in the number of B1 and B2 components with pulsation phase and the stronger scatter in their velocities at three phases from the Cepheid's minimum radius.

The most important point is the behavior of the R component of the Hα line. Its radial velocity remains essentially unchanged, $+32.72 \pm 2.50$ km s^{-1}, except for its slight increase to $+37.17$ km s^{-1} at the phase of the Cepheid's minimum radius (Fig. 9). At this time, the difference in velocities with the B component

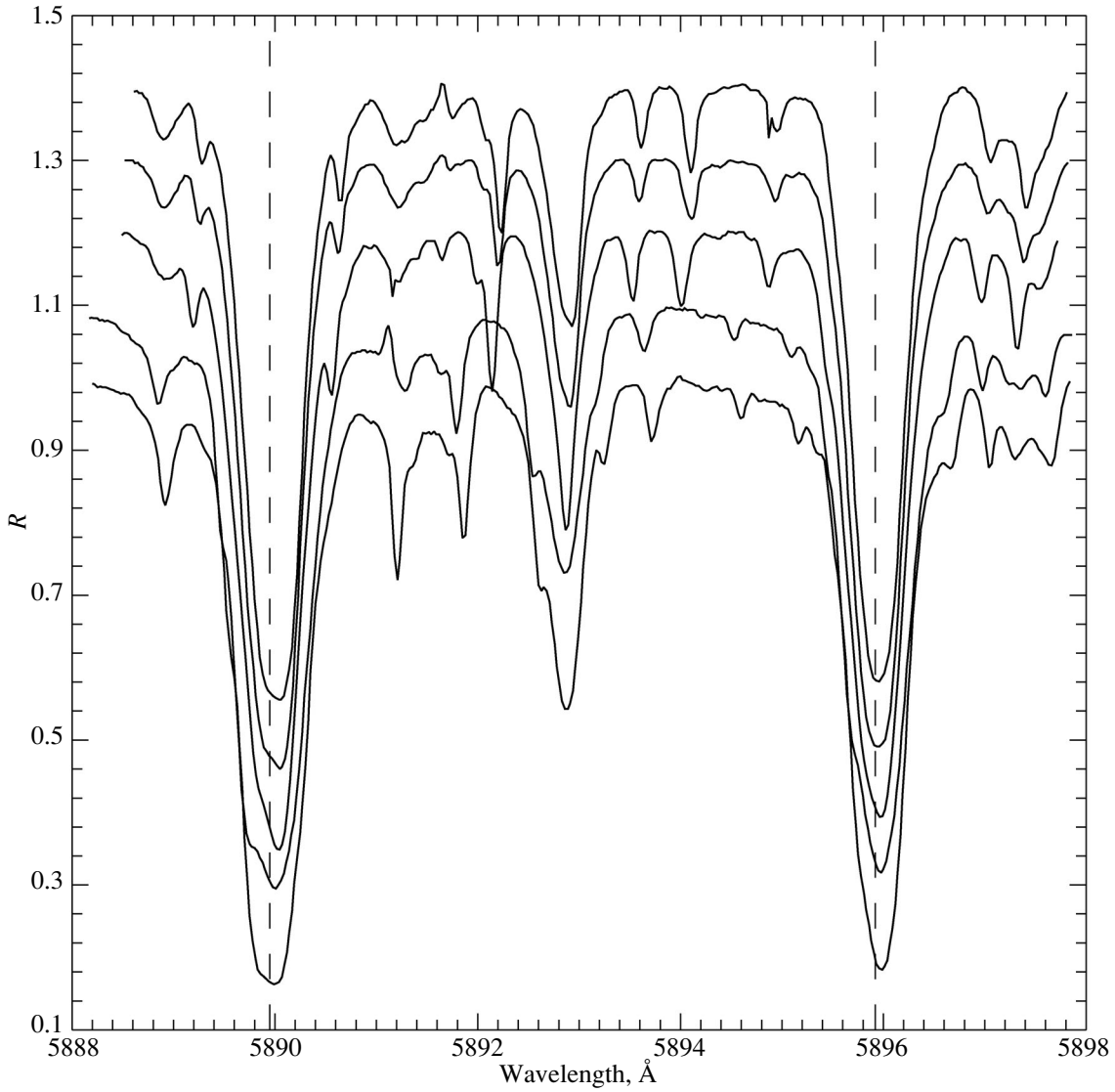

Fig. 6. Changes of the Na I D 5895.932 Å and 5899.297 Å absorption line profiles with increasing pulsation phase (from bottom to top).

reaches a maximum value of 33.08 km s^{-1}, while a slight change in the radial velocity of the Hα core with pulsation phase compared to that determined from the metal lines for Cepheids is one of the indicators of the presence of a circumstellar envelope (Usenko and Klochkova 2015). Hence an important conclusion follows: the R component of the Hα line is formed in the envelope of ζ Gem and is its indicator, because the velocity of this component is not related in any way to the pulsational changes in the supergiant's atmosphere.

The behavior of the R1 and R2 components is more enigmatic. Their number is minimal at the phase of minimum light and the phase of the Cepheid's mean radius and then increases sharply at the phase of its minimum radius. The mean velocity of the R2 components at the phase of minimum light virtually coincides with the velocity of the R component of the Hα line, and these components are farthest in velocity from the R1 components. Subsequently, the velocity difference between these components decreases and remains essentially constant for all the remaining pulsation phases. The scatter in velocities for the R1 components is not as significant as that for the R2 components. The mean velocities of the R1 components also change gradually with pulsation phase, as do those for the B1 and B2 components, and they are probably also

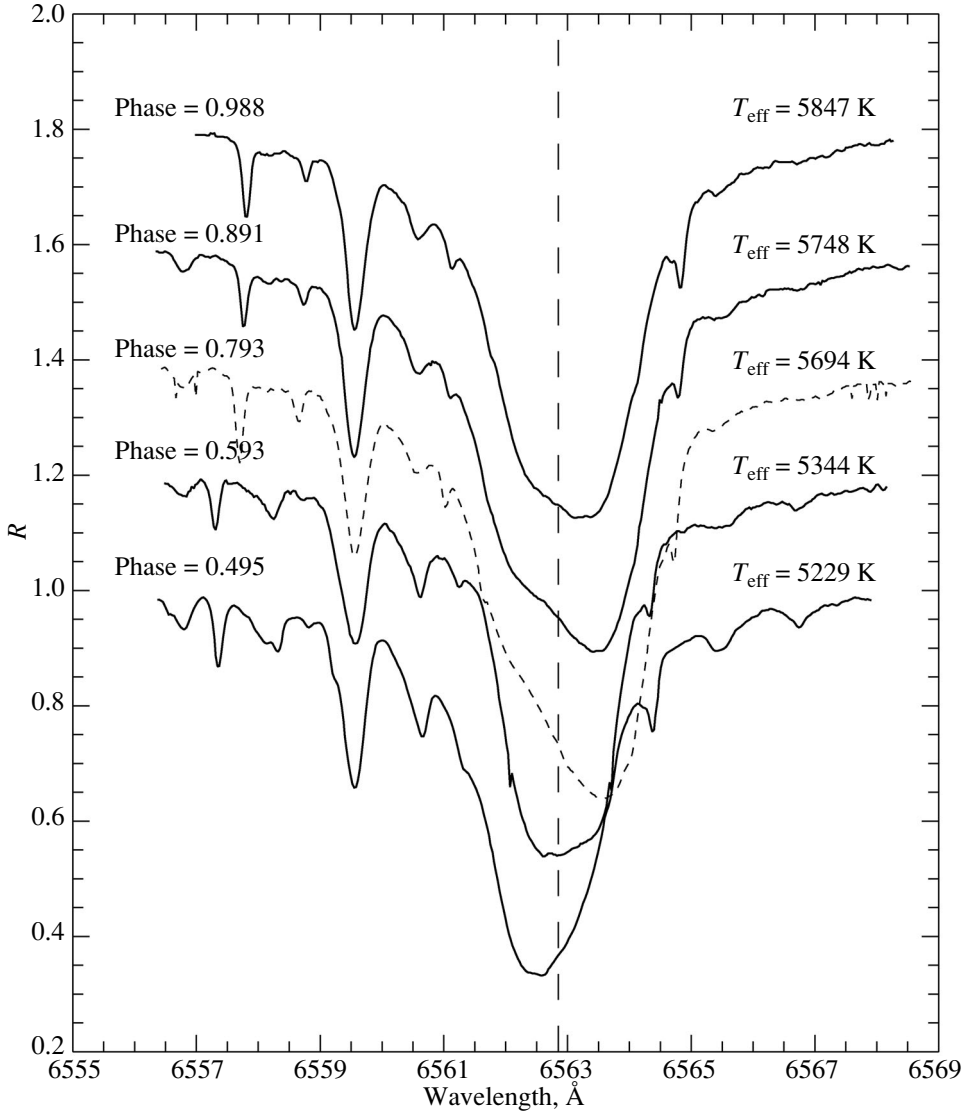

Fig. 7. Changes of the Hα 6562.850 Å absorption line profile with increasing pulsation phase.

formed in the Cepheid's atmosphere. For the R2 components, such changes in the mean velocities are observed only until the phase of minimum radius, whereupon they become almost identical (Fig. 9). Klochkova et al. (2014) showed that the short-wavelength components of lines with low lower-level excitation potentials (most of them are located in the blue spectral range), which differ noticeably in radial velocities from other absorption lines, are formed precisely in the envelope of ρ Cas. As follows from Tables 5–9, in the R2 components, especially for the spectrum at the phase of minimum light, the lines with low $\chi_{\rm low}$ (up to 5.00 eV) constitute the overwhelming majority, but the Si II 6371.355 Å line with $\chi_{\rm low} = 8.12$ eV is present. Therefore, it is rather difficult to state categorically that all R2 components can also be formed in the circumstellar envelope, though the R2 component of the Na I D 5889.966 Å resonance line may well be formed in it.

If the radial velocities estimated from the metal line cores and Hα in this paper are compared with those from Jacobsen and Wallerstein (1982) (see Table 1 and Fig. 1 from their paper) for their 1979–1981 data set, then it can be noticed that the amplitude of the radial velocity curve from the metal lines is slightly smaller (Fig. 9). The radial velocity curve from the Hα core constructed by these authors has an amplitude of ∼36 km s^{-1}. In this paper, as can be seen from Fig. 9, the radial velocities estimated from the Hα line center (crosses) do not differ in any way from

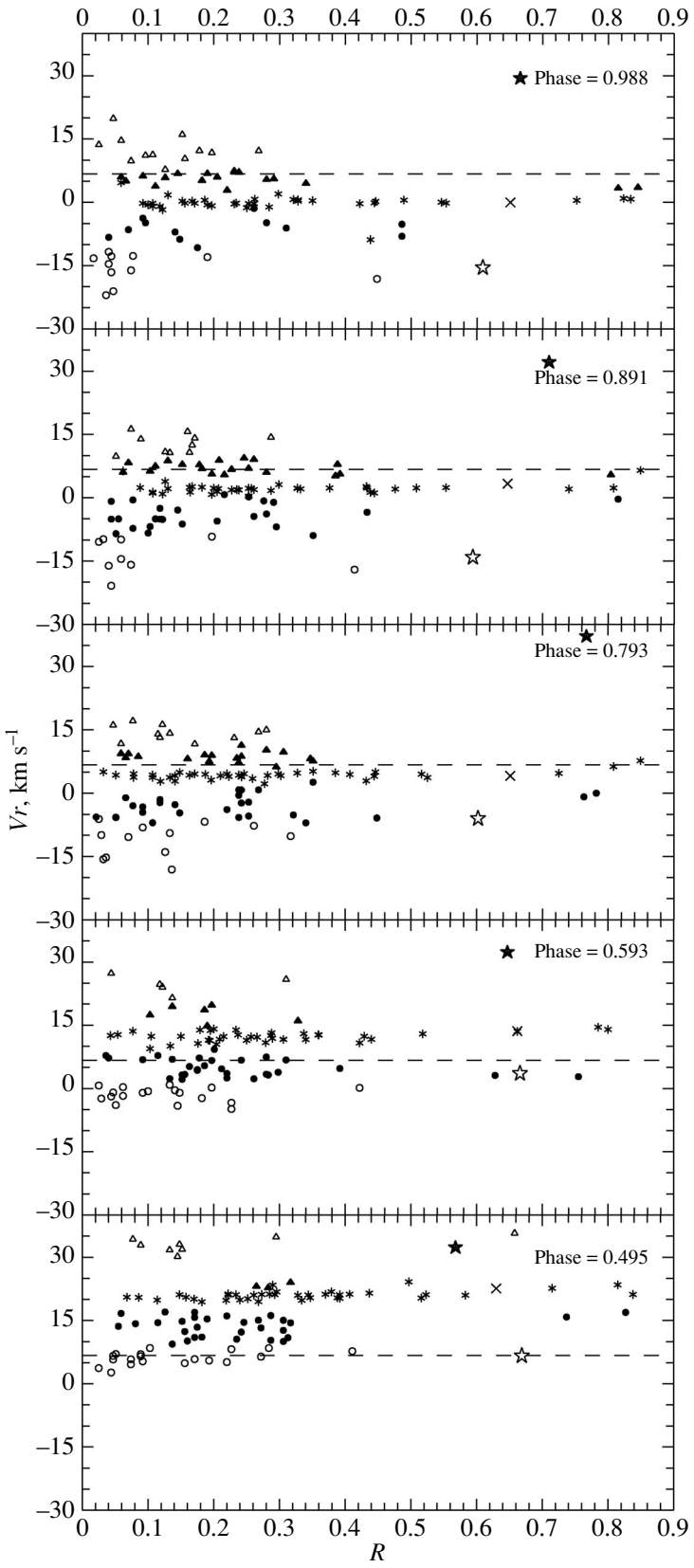

Fig. 8. Radial velocity V_r measured from the cores of the metal absorption lines, their blue (B1, B2) and red (R1, R2) components, the Hα line, and its B and R components versus line depth. The asterisks are the metal lines, the filled circles are the B1 components, the open circles are the B2 components, the filled triangles are the R1 components, the open triangles are the R2 components, the cross is the Hα center, the filled five-point star is the R component, and the open five-point star is the B component. The $\langle V_r \rangle$ estimate is indicated by the dotted line.

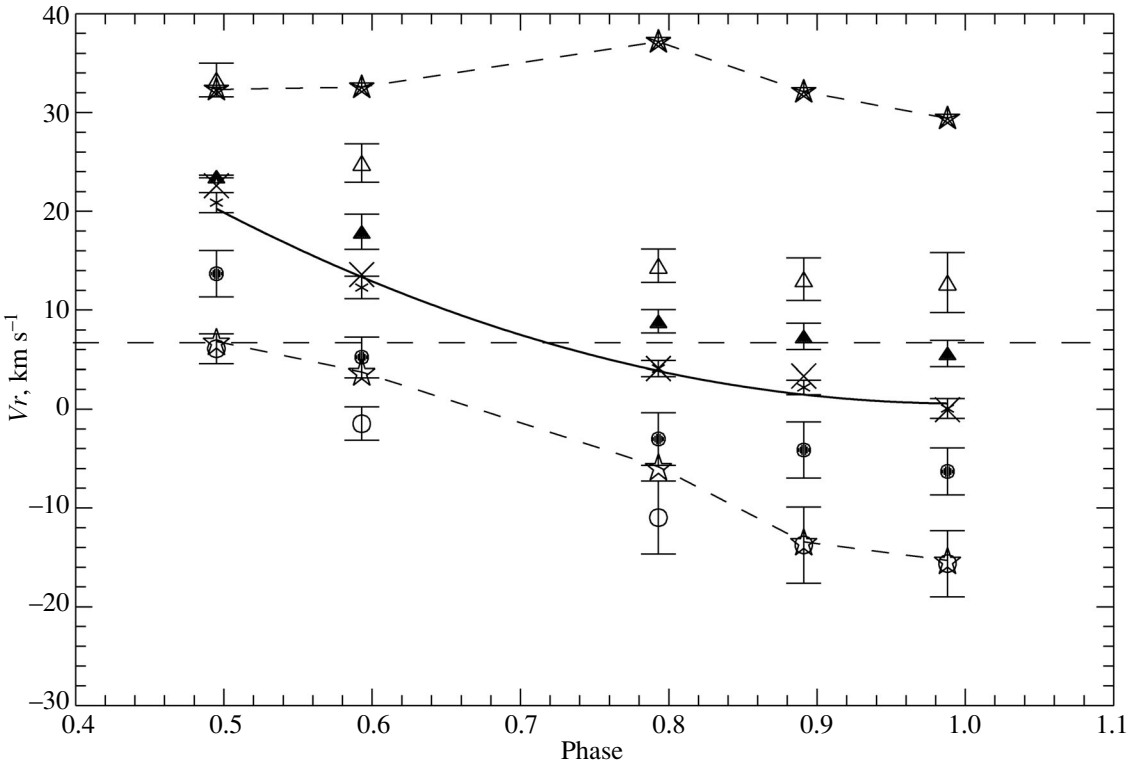

Fig. 9. Averaged estimates of the radial velocity V_r measured from the cores of the metal absorption lines, their blue (B1, B2) and red (R1, R2) components, the Hα line, and its B and R components versus pulsation phase. The designations are the same as those in Fig. 8.

those measured from the metal lines. On the other hand, the difference in the mean velocity estimates obtained from the B and R components of the Hα line is $\sim$37.5 km s^{-1}. Consequently, Jacobsen and Wallerstein (1982) obtained their estimates for the Hα curve by measuring the radial velocities from the dominant B or R component in the line core at a given pulsation phase. Hence a characteristic "shift in phase" arises between the radial velocity curves constructed from the cores of the metal lines and Hα, respectively.

CONCLUSIONS

Through detailed studies of five high-resolution spectra for the classical Cepheid ζ Gem on the ascending branch of the light curve, we estimated its atmospheric parameters, chemical composition, and radial velocities measured from the cores of metal lines, the blue and red components of specially chosen metal lines, and the Hα line. Based on these results, the following conclusions can be reached.

(1) The atmospheric parameters of the Cepheid were refined for each spectrum. Our estimates of the chemical composition show that, according to the abundances of the key elements of the evolution of yellow supergiants, ζ Gem has already passed the first dredge-up and crosses the Cepheid instability strip not for the first time. The abundances of all the remaining elements are nearly solar.

(2) The overwhelming majority of metal absorption lines in the Cepheid's atmosphere show dramatic changes of the shape with pulsation phase, an asymmetry and the formation of blue and red components, often up to two on each side. The Hα absorption line is also split into blue and red components. Such a behavior of the metal and hydrogen absorption lines is observed in Cepheids with circumstellar envelopes (for example, in δ Cep, η Aql, X Sgr, and others).

(3) The radial velocities measured from the cores of the metal absorption lines, their blue B1 and B2 and red R1 and R2 components, and the B and R components of the Hα line showed that their scatter is from -22 to $+36$ km s^{-1} for all pulsation phases but does not exceed 35–40 km s^{-1} for each individual phase. For the B and R components of the Hα line, it does not exceed 22 km s^{-1}.

(4) Based on the radial velocities measured from the cores of the metal lines and their B components at

Table 4. List of anomalous metal lines in the spectra of ζ Gem used to measure the radial velocities

Wavelength	Species	χ_{low}, eV	Wavelength	Species	χ_{low}, eV	Wavelength	Species	χ_{low}, eV
5627.490	Fe II	3.39	6114.690	Zr II	1.66	6432.680	Fe II	2.89
5633.970	Fe I	4.99	6127.912	Fe I	4.14	6475.630	Fe I	2.56
5688.217	Na I	2.10	6175.371	Ni I	4.09	6491.572	Ti II	2.06
5717.838	Fe I	4.28	6179.381	Fe II	5.57	6493.788	Ca I	2.52
5783.069	Cr I	3.32	6226.740	Fe I	3.88	6496.910	Ba II	0.60
5889.966	Na I	0.00	6290.971	Fe I	4.73	6516.080	Fe II	2.89
5895.932	Na I	0.00	6302.503	Fe I	3.69	6518.380	Fe I	2.83
5899.297	Ti I	1.05	6314.670	Ni I	4.15	6533.970	Fe I	4.56
5905.670	Fe I	4.65	6320.400	La II	0.17	6546.248	Fe I	2.76
5916.250	Fe I	2.45	6327.608	Ni I	1.68	6606.951	Ti II	2.06
5956.700	Fe I	0.86	6369.460	Fe II	2.89	6748.834	Ca I	5.89
5991.375	Fe II	3.15	6371.355	Si II	8.12	6767.770	Ni I	1.83
6113.322	Fe II	3.22	6390.480	La II	0.32			

the times of contraction of the Cepheid's atmosphere to its minimum radius and subsequent expansion, we revealed their dependence on the depths of these lines. This may be evidence for the presence of a velocity gradient in the atmosphere. No significant difference in velocities between the atoms and ions of the metal lines is observed, which may also suggest the absence of a significant inhomogeneity in the upper atmospheric layers of ζ Gem.

(5) Since the averaged radial velocities of the B1 and B2 components (and the B components of the Na I D resonance lines), along with the velocities measured from the metal line cores, change with pulsation phase and coincide with the velocities of the B component of the Hα line, we concluded that all these components are formed in the Cepheid's atmosphere. The formation and passage of a shock wave due to the κ-mechanism at work can be responsible for the stronger scatter in their velocities at three phases from the Cepheid's minimum radius and the decrease in the number of these components. The averaged radial velocities of the R1 components also change with pulsation phase and differ only slightly from those determined from the cores of the metal lines and their B1 and B2 components. Consequently, they are also formed in the Cepheid's atmosphere.

(6) The radial velocity of the R component of the Hα line at all pulsation phases is $+32.72 \pm 2.50$ km s^{-1}, changes very little (except for the time of the Cepheid's minimum radius), and differs significantly from the bulk of the velocities. From this it follows that the R component of the Hα line is formed in the envelope of ζ Gem and is an indicator of its presence.

(7) The R2 components of the metal absorption lines behave unusually: the mean velocity of the components at minimum light coincides with the velocity of the R component of the Hα line, it then decreases until the time of minimum radius, whereupon it becomes essentially constant. Given that the overwhelming majority of the lines forming the R2 components have low lower-level excitation potentials, it

Table 5. Radial velocities determined from the anomalous metal lines and their components and their depths in the spectrum at phase $0\overset{P}{.}495$

Wavelength	RV (km s^{-1})									
	B2	r	B1	r	C	r	R1	r	R2	r
5627.490	8.47	0.103	16.09	0.220	23.40	0.290	–	–	–	–
5633.970	4.89	0.156	15.08	0.268	19.18	0.334	–	–	–	–
5688.217	–	–	–	–	21.01	0.583	–	–	35.03	0.295
5717.838	–	–	14.57	0.246	20.41	0.347	–	–	32.12	0.152
5783.069	3.72	0.025	17.01	0.126	20.53	0.158	–	–	–	–
5889.966	–	–	16.93	0.827	21.48	0.838	–	–	35.94	0.658
5895.932	–	–	15.83	0.737	23.48	0.815	–	–	–	–
5899.297	–	–	–	–	19.49	0.268	23.32	0.265	33.27	0.148
5905.670	4.63	0.074	15.36	0.190	21.26	0.285	23.00	0.283	–	–
5916.250	–	–	12.65	0.306	21.83	0.379	–	–	–	–
5956.700	–	–	15.05	0.306	21.10	0.392	–	–	31.96	0.133
5991.375	5.84	0.171	16.18	0.287	21.21	0.370	–	–	–	–
6113.322	6.51	0.089	14.80	0.152	19.89	0.240	–	–	–	–
6114.690	6.60	0.047	16.68	0.059	20.46	0.086	–	–	–	–
6127.912	5.32	0.092	–	–	21.02	0.261	–	–	–	–
6175.371	5.82	0.074	15.73	0.171	20.16	0.252	–	–	–	–
6179.381	5.77	0.047	13.64	0.055	20.54	0.068	–	–	–	–
6226.740	2.66	0.044	14.25	0.081	20.10	0.170	–	–	–	–
6290.971	5.52	0.193	16.94	0.171	21.81	0.296	–	–	–	–
6302.503	6.42	0.272	–	–	20.26	0.392	–	–	–	–
6314.670	–	–	10.57	0.235	20.38	0.388	–	–	–	–
6320.400	–	–	9.40	0.137	21.11	0.239	–	–	–	–
6327.608	–	–	10.99	0.171	21.18	0.273	–	–	–	–
6369.460	–	–	10.16	0.160	21.12	0.293	–	–	–	–
6371.355	–	–	11.06	0.182	21.03	0.222	–	–	34.52	0.077
6390.480	7.06	0.051	14.49	0.115	21.28	0.222	–	–	–	–
6432.680	–	–	10.03	0.306	21.24	0.407	–	–	–	–
6475.630	5.13	0.220	10.92	0.313	20.98	0.328	–	–	–	–
6491.572	–	–	13.24	0.272	21.12	0.148	–	–	–	–
6493.788	8.19	0.227	–	–	21.12	0.523	–	–	–	–
6496.910	7.72	0.411	–	–	22.67	0.715	–	–	–	–
6516.080	–	–	10.31	0.287	24.19:	0.497	24.24	0.317	–	–
6518.380	–	–	14.44	0.317	21.05	0.344	–	–	–	–
6533.970	–	–	13.42	0.175	19.43	0.182	–	–	30.38	0.145
6546.248	8.46	0.284	–	–	20.34	0.516	–	–	–	–
6606.951	–	–	12.40	0.156	19.80	0.219	–	–	33.12	0.089
6748.834	7.01	0.089	–	–	19.87	0.114	–	–	–	–
6767.770	–	–	12.25	0.242	21.50	0.437	–	–	–	–

r is the depth of the lines and their components, RV_{B1}—from the blue B1 line component, RV_{B2}—from the blue B2 line component, RV_C—from the line core, RV_{R1}—from the red R1 line component, RV_{R2}—from the red R2 line component.

Table 6. Radial velocities determined from the anomalous metal lines and their components and their depths in the spectrum at phase $0\overset{P}{.}593$

Wavelength	RV (km s^{-1})									
	B2	r	B1	r	C	r	R1	r	R2	r
5627.490	–	–	3.22	0.152	13.86	0.234	18.85	0.186	–	–
5633.970	−1.01	0.148	–	–	10.89	0.279	–	–	–	–
5688.217	–	–	–	–	12.94	0.518	–	–	26.09	0.310
5717.838	–	–	9.26	0.201	11.88	0.289	–	–	24.92	0.118
5783.069	–	–	2.33	0.133	12.37	0.105	–	–	–	–
5889.966	–	–	2.78	0.755	13.99	0.800	–	–	–	–
5895.932	–	–	3.10	0.628	14.55	0.785	–	–	–	–
5899.297	–	–	5.40	0.186	14.13	0.200	–	–	24.28	0.122
5905.670	0.87	0.133	–	–	12.33	0.215	–	–	–	–
5916.250	–	–	3.55	0.220	12.58	0.287	–	–	–	–
5956.700	–	–	4.65	0.212	13.17	0.288	15.07	0.190	–	–
5991.375	−4.11	0.145	7.44	0.280	12.97	0.337	–	–	–	–
6113.322	−0.42	0.141	7.25	0.178	11.37	0.194	–	–	–	–
6114.690	−2.38	0.029	7.25	0.040	12.78	0.054	–	–	–	–
6127.912	−3.94	0.051	5.21	0.163	13.74	0.195	–	–	–	–
6175.371	–	–	3.32	0.156	10.48	0.204	–	–	–	–
6179.381	0.70	0.025	7.79	0.036	12.57	0.043	–	–	–	–
6226.740	−1.75	0.062	7.79	0.115	9.43	0.103	–	–	–	–
6290.971	−0.65	0.100	6.63	0.197	12.73	0.237	–	–	–	–
6302.503	−4.88	0.227	3.40	0.280	11.65	0.306	–	–	–	–
6314.670	0.22	0.197	–	–	11.60	0.306	–	–	–	–
6320.400	−1.02	0.092	–	–	13.88	0.179	–	–	–	–
6327.608	–	–	2.17	0.152	11.49	0.192	–	–	–	–
6369.460	–	–	4.32	0.175	12.25	0.257	–	–	–	–
6371.355	–	–	4.46	0.175	11.65	0.209	19.67	0.137	27.51	0.044
6390.480	0.34	0.062	–	–	12.34	0.150	–	–	–	–
6432.680	–	–	3.84	0.298	12.69	0.360	–	–	–	–
6475.630	–	–	6.73	0.242	11.43	0.250	–	–	–	–
6491.572	–	–	3.20	0.283	11.61	0.340	–	–	–	–
6493.788	−2.28	0.182	–	–	11.67	0.440	–	–	–	–
6496.910	0.14	0.422	–	–	13.51	0.662	–	–	–	–
6516.080	–	–	2.30	0.261	10.80	0.422	16.27	0.328	–	–
6518.380	–	–	2.47	0.220	12.16	0.266	19.97	0.197	–	–
6533.970	−1.90	0.044	6.91	0.137	10.07	0.134	–	–	21.70	0.137
6546.248	−3.38	0.227	4.75	0.392	12.37	0.429	–	–	–	–
6606.951	–	–	–	–	10.67	0.176	17.67	0.103	–	–
6748.834	−0.96	0.047	6.84	0.092	13.59	0.077	–	–	–	–
6767.770	–	–	6.74	0.310	12.73	0.359	–	–	–	–

r is the depth of the lines and components, RV_{B1}—from the blue B1 line component, RV_{B2}—from the blue B2 line component, RV_C—from the line core, RV_{R1}—from the red R1 line component, RV_{R2}—from the red R2 line component.

Table 7. Radial velocities determined from the anomalous metal lines and their components and their depths in the spectrum at phase $0^P.793$

Wavelength	RV (km s^{-1})									
	B2	r	B1	r	C	r	R1	r	R2	r
5627.490	–	–	–	–	4.28	0.238	7.75	0.193	–	–
5633.970	−9.46	0.133	0.78	0.268	2.23	0.277	–	–	14.21	0.115
5688.217	−7.73	0.261	–	–	3.70	0.525	–	–	15.23	0.280
5717.838	–	–	0.81	0.238	3.43	0.259	8.50	0.235	16.47	0.122
5783.069	−6.14	0.025	−1.10	0.066	3.76	0.078	8.65	0.066	17.35	0.077
5889.966	–	–	−0.88	0.763	7.69	0.849	–	–	–	–
5895.932	–	–	0.01	0.782	6.31	0.808	–	–	–	–
5899.297	–	–	–	–	4.14	0.141	–	–	13.34	0.231
5905.670	–	–	−2.33	0.242	4.60	0.246	7.44	0.238	–	–
5916.250	–	–	−0.53	0.238	3.84	0.242	–	–	13.45	0.118
5956.700	–	–	–	–	4.11	0.210	9.17	0.197	–	–
5991.375	−6.78	0.186	–	–	2.90	0.432	10.47	0.280	–	–
6113.322	−8.13	0.092	–	–	3.94	0.223	–	–	–	–
6114.690	–	–	−5.67	0.021	4.28	0.051	9.61	0.059	–	–
6127.912	–	–	−4.55	0.092	4.56	0.171	8.35	0.160	14.42	0.133
6175.371	–	–	−4.69	0.148	3.11	0.196	–	–	–	–
6179.381	−9.93	0.029	−5.69	0.051	4.59	0.078	–	–	–	–
6226.740	–	–	−5.81	0.051	3.71	0.107	–	–	–	–
6290.971	–	–	−5.76	0.238	5.04	0.032	9.29	0.186	16.35	0.047
6302.503	–	–	0.75	0.242	4.84	0.385	8.95	0.242	–	–
6314.670	–	–	−2.15	0.253	4.21	0.282	6.43	0.295	–	–
6320.400	−10.39	0.070	−2.24	0.118	4.27	0.163	–	–	–	–
6327.608	–	–	−1.51	0.118	3.75	0.133	9.58	0.070	–	–
6369.460	−13.96	0.126	–	–	4.16	0.302	–	–	–	–
6371.355	–	–	−3.90	0.220	4.56	0.298	–	–	–	–
6390.480	−15.65	0.032	−2.98	0.077	4.92	0.148	–	–	–	–
6432.680	–	–	–	–	4.45	0.407	8.41	0.347	–	–
6475.630	–	–	2.60	0.351	5.18	0.351	7.82	0.351	–	–
6491.572	–	–	−5.90	0.448	4.31	0.107	–	–	–	–
6493.788	−10.19	0.317	–	–	4.51	0.516	–	–	–	–
6496.910	−18.10	0.136	–	–	4.69	0.725	–	–	–	–
6516.080	–	–	−7.04	0.340	5.00	0.446	–	–	14.75	0.268
6518.380	–	–	−2.73	0.141	4.56	0.220	11.55	0.242	–	–
6533.970	–	–	–	–	2.81	0.119	8.90	0.085	–	–
6546.248	–	–	−5.18	0.321	4.03	0.444	9.98	0.306	–	–
6606.951	–	–	−3.27	0.092	4.47	0.187	–	–	11.95	0.059
6748.834	−15.25	0.036	−7.01	0.107	2.88	0.141	–	–	–	–
6767.770	–	–	−5.44	0.253	4.79	0.327	–	–	11.89	0.171

r is the depth of the lines and components, RV_{B1}—from the blue B1 line component, RV_{B2}—from the blue B2 line component, RV_C—from the line core, RV_{R1}—from the red R1 line component, RV_{R2}—from the red R2 line component.

Table 8. Radial velocities determined from the anomalous metal lines and their components and their depths in the spectrum at phase $0^P.891$

Wavelength	RV (km s^{-1})									
	B2	r	B1	r	C	r	R1	r	R2	r
5627.490	−9.88	0.059	–	–	2.24	0.253	8.04	0.178	14.13	0.089
5633.970	–	–	−0.75	0.276	1.72	0.287	9.13	0.208	–	–
5688.217	–	–	–	–	2.40	0.553	–	–	14.57	0.287
5717.838	–	–	–	–	2.20	0.257	–	–	10.98	0.163
5783.069	–	–	−5.02	0.055	1.34	0.107	6.28	0.062	–	–
5889.966	–	–	−0.33	0.815	6.50	0.849	–	–	–	–
5895.932	–	–	–	–	2.32	0.808	5.67	0.804	–	–
5899.297	–	–	–	–	3.89	0.126	–	–	14.36	0.171
5905.670	–	–	−5.01	0.111	1.84	0.238	8.11	0.152	–	–
5916.250	–	–	0.23	0.253	0.38	0.253	7.14	0.182	–	–
5956.700	–	–	–	–	2.17	0.207	–	–	11.09	0.126
5991.375	–	–	−3.85	0.280	2.65	0.432	–	–	10.91	0.133
6113.322	−9.22	0.197	–	–	1.91	0.261	5.87	0.197	–	–
6114.690	−10.45	0.025	−0.85	0.044	6.33	0.062	–	–	10.07	0.051
6127.912	–	–	−5.09	0.118	2.51	0.182	–	–	16.48	0.074
6175.371	–	–	−6.22	0.152	0.78	0.197	–	–	–	–
6179.381	−9.82	0.032	−0.52	0.077	2.38	0.088	–	–	–	–
6226.740	–	–	−8.50	0.051	1.11	0.107	–	–	–	–
6290.971	–	–	−4.40	0.261	1.95	0.235	–	–	–	–
6302.503	–	–	−1.10	0.291	2.31	0.376	5.42	0.385	–	–
6314.670	–	–	–	–	1.85	0.227	6.97	0.227	–	–
6320.400	–	–	−6.83	0.103	2.62	0.167	–	–	–	–
6327.608	−16.12	0.040	−2.52	0.118	2.16	0.130	7.73	0.111	–	–
6369.460	−14.51	0.059	–	–	2.29	0.327	–	–	–	–
6371.355	–	–	−5.52	0.205	2.11	0.332	6.24	0.280	–	–
6390.480	−20.85	0.044	−8.36	0.100	2.45	0.163	6.51	0.103	–	–
6432.680	–	–	−8.96	0.351	2.30	0.433	5.67	0.216	–	–
6475.630	–	–	0.75	0.216	3.10	0.299	9.61	0.246	–	–
6491.572	–	–	−3.42	0.433	1.15	0.444	8.14	0.388	–	–
6493.788	–	–	−6.90	0.295	2.32	0.508	9.31	0.261	–	–
6496.910	−17.03	0.414	–	–	2.07	0.740	–	–	–	–
6516.080	–	–	–	–	2.05	0.476	–	–	15.89	0.160
6518.380	–	–	−7.26	0.077	1.46	0.205	–	–	12.73	0.167
6533.970	–	–	−5.07	0.044	0.92	0.122	8.54	0.070	–	–
6546.248	–	–	–	–	1.31	0.438	5.83	0.392	–	–
6606.951	–	–	−5.12	0.122	2.28	0.200	9.01	0.130	–	–
6748.834	−15.89	0.074	−2.92	0.145	1.33	0.164	–	–	–	–
6767.770	–	–	–	–	2.21	0.327	7.16	0.253	–	–

r is the depth of the lines and components, RV_{B1}—from the blue B1 line component, RV_{B2}—from the blue B2 line component, RV_C—from the line core, RV_{R1}—from the red R1 line component, RV_{R2}—from the red R2 line component.

Table 9. Radial velocities determined from the anomalous metal lines and their components and their depths in the spectrum at phase $0^P.988$

Wavelength	RV (km s^{-1})									
	B2	r	B1	r	C	r	R1	r	R2	r
5627.490	−11.73	0.040	–	–	0.73	0.262	–	–	11.50	0.107
5633.330	–	–	−7.04	0.141	−1.12	0.284	3.09	0.220	–	–
5688.217	–	–	–	–	−0.18	0.553	–	–	12.43	0.268
5717.838	–	–	–	–	−0.32	0.253	–	–	10.56	0.156
5783.069	–	–	–	–	−0.57	0.100	6.21	0.059	–	–
5889.966	–	–	–	–	0.76	0.834	3.74	0.845	–	–
5895.932	–	–	–	–	0.92	0.823	3.58	0.815	–	–
5899.297	–	–	–	–	1.73	0.130	–	–	11.97	0.197
5905.670	–	–	–	–	−0.18	0.234	–	–	8.00	0.126
5916.250	–	–	−1.46	0.261	−1.29	0.250	5.39	0.182	–	–
5956.700	–	–	–	–	0.50	0.186	–	–	11.34	0.096
5991.375	–		−6.10	0.310	−8.85	0.438	7.67	0.231	–	–
6113.322	−16.12	0.074	–	–	−0.29	0.261	–	–	–	–
6114.690	−13.26	0.017	–	–	4.65	0.059	–	–	13.89	0.025
6127.912	–	–	–	–	0.27	0.167	6.08	0.126	14.87	0.059
6175.371	–	–	−8.74	0.148	−0.82	0.197	–	–	20.09:	0.047
6179.381	−12.77	0.044	–	–	−0.26	0.092	–	–	–	–
6226.740	−21.07	0.047	−6.47	0.070	−0.94	0.107	–	–	–	–
6290.971	–	–	−4.84	0.280	−0.38	0.231	7.02	0.145	–	–
6302.503	–	–	–	–	0.29	0.328	4.70	0.340	–	–
6314.670	–	–	–	–	−0.22	0.261	7.03	0.190	–	–
6320.400	–	–	−8.31	0.040	−0.20	0.156	6.45	0.092	–	–
6327.608	−14.61	0.040	−3.76	0.092	−0.96	0.118	–	–	–	–
6369.460	−12.72	0.077	–	–	0.59	0.328	–	–	–	–
6371.355	–	–	−10.74	0.175	0.38	0.350	–	–	–	–
6390.480	−22.00	0.036	–	–	0.29	0.152	4.04	0.111	–	–
6432.680	–	–	–	–	0.21	0.446	5.80	0.291	–	–
6475.630	–	–	–	–	1.96	0.298	7.36	0.238	–	–
6491.572	−13.00	0.190	−5.20	0.486	−0.11	0.444	–	–	–	–
6493.788	–	–	−8.05	0.486	0.02	0.546	–	–	–	–
6496.910	−18.14	0.448	–	–	0.48	0.752	–	–	–	–
6516.080	–	–	–	–	0.51	0.489	–	–	16.28	0.152
6518.380	–	–	–	–	−0.26	0.107	–	–	12.45	0.178
6533.970	–	–	–	–	−1.76	0.122	5.29	0.066	–	–
6546.248	–	–	–	–	−0.31	0.422	5.63	0.280	–	–
6606.951	–	–	–	–	−0.61	0.190	–	–	10.04	0.074
6748.834	−16.59	0.044	−4.88	0.096	−0.21	0.171	–	–	–	–
6767.770	–	–	–	–	0.67	0.321	6.23	0.205	–	–

r is the depth of the lines and components, RV_{B1}—from the blue B1 line component, RV_{B2}—from the blue B2 line component, RV_C—from the line core, RV_{R1}—from the red R1 line component, RV_{R2}—from the red R2 line component.

can be hypothesized that these components can also be formed in the Cepheid's envelope.

(8) All the above features of the spectra for ζ Gem are consistent with the main signatures of circumstellar envelopes around Cepheids described by Usenko and Klochkova (2015). The main conclusion follows from this: the Cepheid has a circumstellar envelope whose presence was previously assumed by Schmidt and Parsons (1984) and Deasy (1988).

ACKNOWLEDGMENTS

This study was financially supported by the Swiss National Science Foundation SCOPES (project no. IZ73Z0152485). I am grateful to B.W. Carney for the provided spectroscopic material, to V.G. Klochkova for her help and useful discussions, and to V.V. Kovtyukh for his help in preparing the paper.

REFERENCES

1. P. Barmby, M. Marengo, N. R. Evans, G. Bono, D. Huelsman, K. Y. L. Su, D. L. Welch, and G. G. Fazio, Astron. J. **141**, 42 (2011).
2. L. N. Berdnikov, A. Yu. Knyazev, I. A. Usenko, V. V. Kovtyukh, and V. V. Kravtsov, Astron. Lett. **36**, 490 (2010).
3. H. P. Deasy, Mon. Not. R. Astron. Soc. **231**, 673 (1988).
4. A. M. Fry and B. W. Carney, Astron. J. **113**, 1073 (1997).
5. A. M. Fry and B. W. Carney, Astron. J. **118**, 1806 (1999).
6. G. A. Galazutdinov, Preprint SAO RAN, № 92, 1 (1992).
7. A. Gallenne, P. Kervella, and A. Mérand, Astron. Astrophys. **538**, 24 (2012).
8. T. S. Jacobsen and G. Wallerstein, Publ. Astron. Soc. Pacif. **94**, 471 (1982).
9. P. Kervella and A. Dominicano de Souza, Astron. Astrophys. **453**, 1059 (2006).
10. P. N. Kholopov, N. N. Samus', M. S. Frolov, et al., *General Catalogue of Variable Stars* (Nauka, Moscow, 1986), Vol. 3 [in Russian].
11. L. L. Kiss, Mon. Not. R. Astron. Soc. **297**, 825 (1998).
12. V. G. Klochkova, V. E. Panchuk, N. S. Tavolzhanskaya, and I. A. Usenko, Astron. Rep. **58**, 101 (2014).
13. V. V. Kovtyukh, Mon. Not. R. Astron. Soc. **378**, 617 (2007).
14. V. V. Kovtyukh and S. M. Andrievsky, Astron. Astrophys. **351**, 597 (1999).
15. R. L. Kurucz, in *Proceedings of the 149th IAU Symposium on Stellar Populations of Galaxies, Angra dos Reis, Brazil, August 5–9, 1991,* Ed. by B. Barbuy and A. Renzini (Kluwer Academic, Dordrecht, 1992), p. 225.
16. R. E. Luck, S. M. Andrievsky, A. B. Fokin, and V. V. Kovtyukh, Astron. J. **136**, 98 (2008).
17. P. Mathias, D. Gillet, A. B. Fokin, N. Nardetto, P. Kervella, and D. Mourard, Astron. Astrophys. **457**, 575 (2006).
18. A. Mérand, P. Kervella, V. Coudé de Foresto, G. Perrin, S. T. Ridgway, J. P. Aufdenberg, T. A. ten Brummelaar, H. A. McAlister, et al., Astron. Astrophys. **453**, 155 (2006).
19. A. Mérand, J. P. Aufdenberg, P. Kervella, V. Coudé du Foresto, T. A. ten Brummelaar, H. A. McAlister, L. Sturmann, J. Sturmann, and N. H. Turner, Astrophys. J. **664**, 1093 (2007).
20. N. Nardetto, J. H. Groth, S. Kraus, F. Millour, and D. Gillet, Astron. Astrophys. **489**, 1263 (2008).
21. A. W. Rogers and R. A. Bell, Mon. Not. R. Astron. Soc. **135**, 121 (1967a).
22. A. W. Rogers and R. A. Bell, Mon. Not. R. Astron. Soc. **136**, 91 (1967b).
23. G. Russo and C. Sollazzo, Inform. Bull. Var. Stars **1807**, 1 (1980).
24. D. D. Sasselov and J. B. Lester, Astrophys. J. **362**, 333 (1990).
25. E. G. Schmidt, Astrophys. J. **162**, 871 (1970).
26. E. G. Schmidt and S. B. Parsons, Astrophys. J. **279**, 202 (1984).
27. I. A. Usenko and V. G. Klochkova, Astron. Lett. **41**, 351 (2015).
28. I. A. Usenko, A. Yu. Knyazev, L. N. Berdnikov, and V. V. Kravtsov, A. B. Fokin, Astron. Lett. **39**, 432 (2013).
29. I. A. Usenko, A. Yu. Knyazev, L. N. Berdnikov, A. B. Fokin, and V. V. Kravtsov, Astron. Lett. **40**, 435 (2014a).
30. I. A. Usenko, A. Yu. Knyazev, L. N. Berdnikov, and V. V. Kravtsov, I. A. Usenko et al., Astron. Lett. **40**, 800 (2014b).
31. R. Wielen, H. Schwan, C. Dettbarn, H. Lendhardt, H. Jahreiss, and H. Jahrling, Veroeff. Astron. Rehen-Inst. Heidelberg **35**, 1 (1999).

Translated by V. Astakhov